JBC RESEARCH ARTICLE

Uncoupling the BMP receptor antagonist function from the WNT agonist function of R-spondin 2 using the inhibitory peptide dendrimer RW^{d}

Received for publication, October 13, 2021, and in revised form, January 4, 2022 Published, Papers in Press, January 12, 2022,
https://doi.org/10.1016/j.jbc.2022.101586

Hyeyoon Lee[1,‡], **Rui Sun**[1,‡], **and Christof Niehrs**[1,2,*]

From the [1]*Division of Molecular Embryology, DKFZ-ZMBH Alliance, Deutsches Krebsforschungszentrum (DKFZ), Heidelberg, Germany;* [2]*Institute of Molecular Biology (IMB), Mainz, Germany*

Edited by Eric Fearon

Signaling by bone morphogenetic proteins (BMPs) plays pivotal roles in embryogenesis, adult tissue homeostasis, and disease. Recent studies revealed that the well-established WNT agonist R-spondin 2 (RSPO2) is also a BMP receptor (BMP receptor type 1A) antagonist, with roles in early *Xenopus* embryogenesis and human acute myeloid leukemia (AML). To uncouple the BMP antagonist function from the WNT agonist function and to promote development of AML therapeutics, here we identified a 10-mer peptide (RW) derived from the thrombospondin 1 domain of RSPO2, which specifically prevents binding between RSPO2 and BMP receptor type 1A without altering WNT signaling. We also show that a corresponding RW dendrimer (RW^{d}) exhibiting improved half-life relieves inhibition of BMP receptor signaling by RSPO2 in human AML cells, reduces cell growth, and induces differentiation. Moreover, microinjection of RW^{d} in *Xenopus* embryos ventralizes the dorsoventral embryonic patterning by upregulating BMP signaling without affecting WNT signaling. Our study corroborates the function of RSPO2 as a BMP receptor antagonist and provides a proof of concept for pharmacologically uncoupling BMP antagonist from WNT agonist functions of RSPO2 using the inhibitor peptide RW^{d} with enhanced target selectivity and limited side effects.

Bone morphogenetic proteins (BMPs) are transforming growth factor beta family of growth factors with diverse roles in embryonic development and adult tissue homeostasis. Their misregulation is implicated in various diseases, including cancer (1–5). Thus, clinical therapies targeting BMP signaling attract great interest (6).

BMPs initiate signaling from a tetrameric receptor kinase complex consisting of type I (BMP receptor type 1A (BMPR1A), BMP receptor type 1B, activin A receptor type I (ACVR1), or activin A receptor–like type I) and type II receptors (BMPR2, ACVR2A, and ACVR2B) (7) in a combinatorial manner (8). Activated BMP receptors phosphorylate small mothers against decapentaplegic 1 (SMAD1), SMAD5, and SMAD8, which enter the nucleus in cooperation with SMAD4 to regulate gene expression (9, 10) and activate Erk, c-Jun N-terminal kinase/P38, or PI3K/Akt mitogen-activated protein (MAP) kinases (MAPKs) (11, 12). A number of extracellular antagonists of BMP signaling are known, which target ligand or receptor activation to modulate amplitude of the signaling (13). Recently, we found that the well-characterized WNT agonists of the R-spondin (RSPO) class have a dual role as BMP receptor antagonist (14).

RSPO1–4 are a family of secreted stem cell growth factors involved in embryonic development, stem cell maintenance, and cancer (15–21). Mechanistically, RSPOs activate WNT signaling by preventing frizzled/lipoprotein receptor–related protein (LRP)5/6 WNT receptor ubiquitination and degradation mediated *via* the transmembrane E3 ubiquitin ligases ring finger 43 (RNF43) and zinc and ring finger 3 (ZNRF3) (17, 22–24). To do so, RSPOs bind to ZNRF3/RNF43 in conjunction with the stem cell marker leucine-rich repeat containing G protein–coupled receptor 5 (LGR5), or two related proteins, LGR4 and LGR6, leading to the internalization of the RSPO–LGR–ZNRF3/RNF43 complex and lysosomal degradation (16, 17, 25). We showed that among the four RSPOs, only RSPO2 and RSPO3 are bifunctional, activating WNT signaling and inhibiting BMP signaling. Mechanistically, RSPO2 specifically interacts with BMPR1A and tethers it to ZNRF3 in an LGR-independent manner to trigger endocytosis and degradation of BMPR1A (14, 26).

In vivo support for a role of RSPO2 as selective BMP antagonist comes from early *Xenopus* embryogenesis, where RSPO2 cooperates with other BMP antagonists of the Spemann organizer to inhibit BMP signaling during embryonic axis formation (14). RSPO2 functions as BMP antagonist rather than WNT agonist also in acute myeloid leukemia (AML) cells, where RSPO2 promotes self-renewal (26). Moreover, in AML patients, elevated *RSPO2* expression is a prognostic marker that strongly correlates with poor disease progression. Thus, RSPO2 is a promising therapeutic target in AML, the more so as it is accessible to extracellularly acting drugs. Indeed, monoclonal antibody antagonists of RSPO family members are effective in inhibiting tumor growth in various solid tumor xenograft models (15). However, a caveat of bulky antibody antagonists is that they are likely to inhibit

‡ These authors contributed equally this work.
* For correspondence: Christof Niehrs, niehrs@dkfz-heidelberg.de.

both WNT agonist and BMP antagonist function of RSPO2 and RSPO3, thus compromising their specificity.

We therefore sought to identify an inhibitor that would specifically target the BMP antagonist ($RSPO2^{BMP}$) but not WNT agonist ($RSPO2^{WNT}$) function of RSPO2. RSPOs harbor two furin-like repeat (FU1 and FU2) domains that engage ZNRF3/RNF43 and LGRs, respectively (16, 27, 28). C-terminally, they contain a thrombospondin 1 (TSP1) domain that mediates binding to heparan sulfate proteoglycans and promotes WNT5A/planar cell polarity signaling (29), but that is largely dispensable for WNT/LRP6 signaling (30–32). The key insight toward a BMP-specific inhibitor was our observation that RSPOs binds BMPR1A *via* its TSP1 domain (14). Building on this observation, we identified a 10-mer peptide (RW) derived from the RSPO2 TSP1 domain, which binds BMPR1A and competes RSPO2 binding. A RW peptide dendrimer (RW^d) neutralizes the RSPO2-mediated decrease of BMP4 signaling without affecting WNT/β-catenin signaling. In THP-1 AML cells, RW^d upregulates BMP signaling, induces cell differentiation, and inhibits cell growth independent of WNT signaling. Finally, administration of RW^d to *Xenopus* embryos increases BMP signaling and induces ventralization during dorsoventral axis formation without affecting WNT signaling. Our study corroborates the RSPO2–BMP4 antagonism and provides a proof of concept that BMP antagonism and WNT agonism can be uncoupled by specific pharmacological intervention with the TSP1 domain of RSPO2 ($RSPO2^{TSP1}$)–BMPR1A binding.

Results

Identification of a $RSPO2^{TSP1}$ domain–derived peptide targeting RSPO2–BMPR1A

Building on the specific interaction of $RSPO2^{TSP1}$ with BMPR1A, we wondered whether a peptide derived from $RSPO2^{TSP1}$ may compete with RSPO2 for BMPR1A binding (Fig. 1*A*). To this end, we scanned the TSP1 domain designing 11 overlapping 10 to 13 mer peptides derived from human $RSPO2^{TSP1}$ (Fig. 1*B*). We set up a solid-phase binding assay with immobilized $RSPO2^{TSP1}$ to which was added a fusion protein of alkaline phosphatase (AP) and the $BMPR1A^{ECD}$ (extracellular domain). We then tested the TSP1-derived peptides as competitors, monitoring inhibition of AP-$BMPR1A^{ECD}$ binding to RSPO2 in the solid-phase binding assay. At 100 μM, treatment with peptides RW (RNNRTSGFKW), DE (DTILSPTIAE), and SG (SRRSKMTMRHSPG) reduced the $RSPO2^{TSP1}$–$BMPR1A^{ECD}$ interaction greater than 50% (Fig. 1, *C* and *D*). Since RW was the most potent peptide, we focused on it and confirmed that it inhibited $RSPO2^{TSP1}$–$BMPR1A^{ECD}$ binding with an IC_{50} ≈40 μM (Fig. 1*E*). The RW sequence is only partially conserved in other RSPOs (Fig. 1*F*). An *in vitro* binding assay with biotinylated RW peptide confirmed that it binds $BMPR1A^{ECD}$ directly (Fig. 1, *G* and *H*). We conclude that RW peptide derived from $RSPO2^{TSP1}$ is a pseudoligand of BMPR1A that competes with RSPO2 for BMPR1A binding.

Monomeric RW peptide has low stability

Low storage stability and short half-life *in vivo* are known disadvantages of monomeric peptides (33–35). Indeed, we found that storage of reconstituted RW monomer reduces its ability to inhibit RSPO2–BMPR1A binding (Fig. S1*A*). To retain peptide stability, we tested covalent attachment of PEG to both N and C terminus of the peptide (PEG-RW) (36). TK peptide, which showed no effect on RSPO2–BMPR1A interaction (Fig. 1, *D* and *G*), was also PEGylated and utilized as a control (PEG-TK). However, in cell surface–binding assays (Fig. S1, *B*–*D*), PEGylation of monomeric RW proved ineffective, since PEG-RW inhibited RSPO2–BMPR1A interaction only upon short-term (3 h) but not during long-term (16 h) treatment (Fig. S1, *C* and *D*).

Dendrimerized RW peptide retains stability and disrupts RSPO2–BMPR1A interaction

As alternative to PEGylation, we considered peptide oligomerization in peptide dendrimers, known to strengthen target binding by enhancing avidity (37) and to provide improved resistance to proteases (38, 39). Therefore, we tested RW dendrimers where individual peptide monomers are assembled on an octavalent lysine core matrix, forming an 8-mer complex with expected size of ∼12 kDa. MiniPEG was either added to the N terminus of the RW dendrimer (N-PEG-RW^d) or inserted as a linker between peptide monomer and core matrix (C-PEG-RW^d) (Fig. 2*A*). As controls, we employed corresponding KR peptide derivatives, which did not affect RSPO2–BMPR1A interaction *in vitro* (Fig. S2*A*). To test whether RW dendrimer retains stability and ability to disrupt the RSPO2–BMPR1A interaction, we performed cell surface–binding assays in cells transfected with BMPR1A or with LGR4 that binds to the FU2 instead of the TSP1 domain (16) (Fig. 2*B*). Three-hour exposure to 20 μM RW^d and N-PEG RW^d abolished RSPO2 binding to BMPR1A transfected cells, whereas KR^d and N-PEG KR^d showed no effect (Fig. 2, *C*–*F*). RW^d and N-PEG RW^d were equally effective, indicating that PEGylation does not affect the efficacy of dendrimerized RW. Unlike monomeric RW peptide, 16 h of RW^d and N-PEG RW^d treatment was still able to completely disrupt RSPO2–BMPR1A binding (Fig. S2, *B* and *C*). Interestingly, 20 μM RW^d was unable to abolish RSPO3 binding to BMPR1A transfected cells (Fig. 2, *G* and *H*). Altogether, these results suggest that RW peptide dendrimer is stable and potently competes the RSPO2–BMPR1A interaction without affecting LGR4 binding, which is required for WNT signal activation.

RW dendrimer derepresses BMP4–BMPR1A signaling

Given that RSPO2 antagonizes BMP4 signaling (14, 26), we expected that RW^d derepresses RSPO2-mediated inhibition of BMP4 signaling. To test this prediction, we employed human hepatocellular carcinoma (HEPG2) cells, which harbor very low endogenous RSPO2 expression (14). BMP4 induced Smad1 phosphorylation (pSmad1), a hallmark of BMP signaling activation, and RSPO2 treatment inhibited this

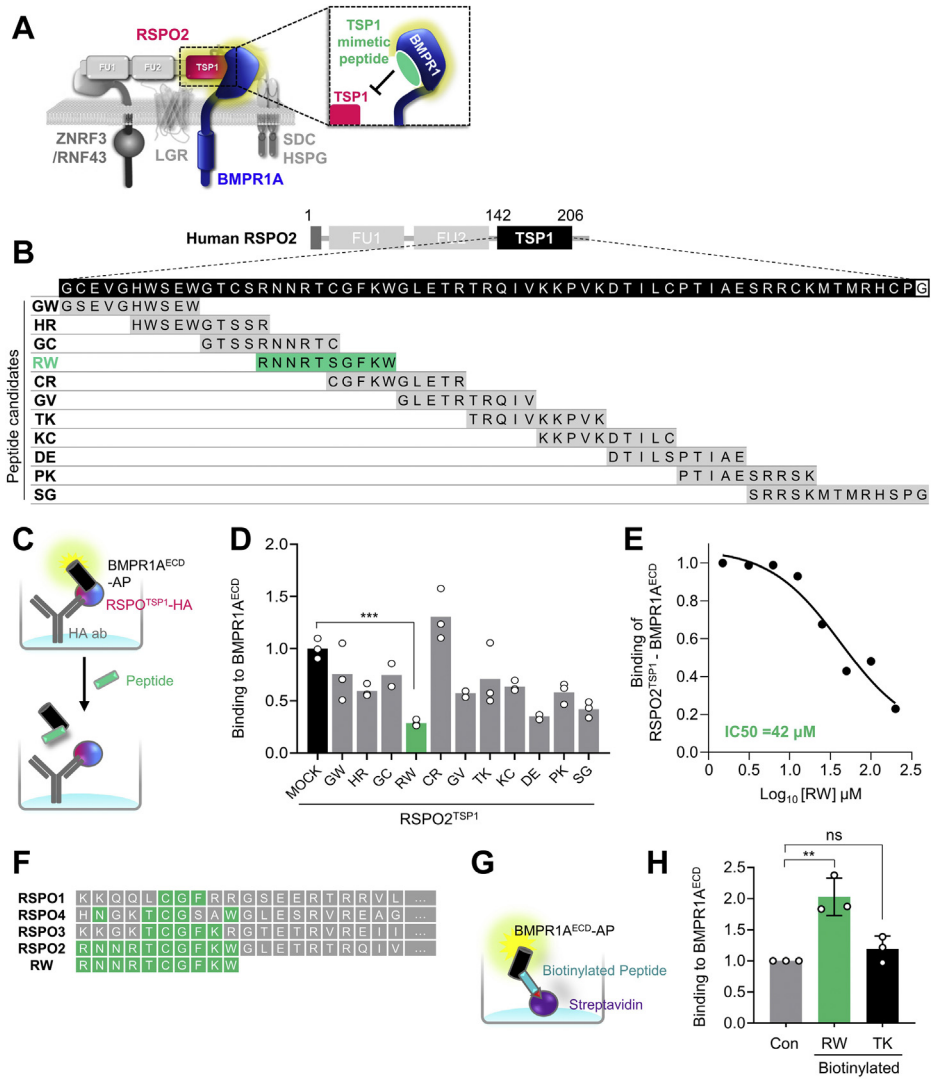

Figure 1. Design and validation of peptide to block RSPO2–BMPR1A interaction. *A*, scheme for design of RSPO2^{TSP1}-derived peptide to block RSPO2 access to BMPR1A^{ECD} for interaction. *B*, amino acid sequence of human RSPO2^{TSP1} domain (amino acids 142–206; *black boxes*) and overlapping peptide candidates derived from the TSP1 domain. About 11 peptides consisting of 10 to 14 amino acids were designed with 5 mer offset. Designated names of corresponding peptides are indicated on the *left side*. Note that cysteine residues in the *middle* of each peptide were exchanged into serine residues for synthesis. *C*, scheme for *in vitro* competitive binding assay of (*D*). HA-fused RSPO2^{TSP1} were treated on anti-HA antibody-coated plate as baits, followed by AP-fused BMPR1A^{ECD} treatment for 3 h with or without 100 μM of peptide candidates. Binding between RSPO2^{TSP1} and BMPR1A^{ECD} was detected with AP activity. *D*, *in vitro* binding assay for RSPO2^{TSP1} and BMPR1A^{ECD} interaction competing with overlapping peptides. Note that RW peptide exhibited the strongest inhibition for RSPO2^{TSP1}–BMPR1A binding. n = 2 to 3 experimental replicates. Data are displayed as means ± SD. ns; ***$p < 0.001$ from two-tailed unpaired *t* test. *E*, IC_{50} curve for RW peptide to inhibit RSPO2^{TSP1}–BMPR1A^{ECD} interaction. Note that IC_{50} of RW for RSPO2^{TSP1}–BMPR1A^{ECD} is 42 μM. *F*, amino acid sequence alignment of human RSPO1–4 with RW peptide. Conserved amino acids are indicated with *green boxes*. *G*, scheme for *in vitro* binding assay to analyze direct binding between RW peptide and BMPR1A^{ECD} in (*G*). Biotinylated RW or TK peptide was treated on streptavidin-coated plate as a bait, followed by BMPR1A^{ECD}–AP treatment. Binding of peptide-BMPR1A^{ECD} was detected with AP activity. *H*, *in vitro* binding assay showing direct RW and BMPR1A^{ECD} interaction. n = 3 experimental replicates. Data are displayed as means ± SD. ns; **$p < 0.01$ from two-tailed unpaired *t* test. AP, alkaline phosphatase; BMPR1A, BMP receptor type 1A; BMPR1A^{ECD}, extracellular domain of BMPR1A; FU, furin domain; HSPG, heparin sulfate proteoglycan; ns, not significant; RSPO2, R-spondin 2; RSPO2^{TSP1}, TSP1 domain of RSPO2; SDC, syndecan; TSP1, thrombospondin 1 domain.

activation, as previously described (Fig. 3*A*) (14). Importantly, RW^{d} but not KR^{d} rescued the RSPO2-mediated but not the RSPO3-mediated decrease of pSmad1 levels, suggesting that RW^{d} specifically impairs the BMP antagonist function of RSPO2 (Fig. 3, *A* and *B*). Administration of RW^{d} without simultaneous treatment of RSPO2 showed no effect on pSmad1 level in HEPG2 cells (Fig. 3*C*). This result supports that RW^{d} acts *via* RSPO2 to modulate BMP signaling. To corroborate this finding, we tested RW^{d} on human lung carcinoma (H1581) cells, which express elevated levels of *RSPO2* (14). Strikingly, RW^{d} increased phosphorylation of Smad1 similar to *RSPO2* deficiency (14, 26) (Fig. 3*D*). BMP signaling activation is also known to induce phosphorylation of MAPKs, referred as a non-Smad1 BMP signaling (11, 12, 40, 41). Therefore, we analyzed whether RW^{d} derepresses RSPO2-mediated inhibition of MAPK phosphorylation. BMP4 induced P38 MAPK and P44/42 MAPK phosphorylation (pP38 and pP44/42), and RSPO2 treatment disrupted this activation. Similar to Smad1-dependent BMP4 signaling, RW^{d} but not KR^{d} rescued the RSPO2-mediated decrease of pP38 and

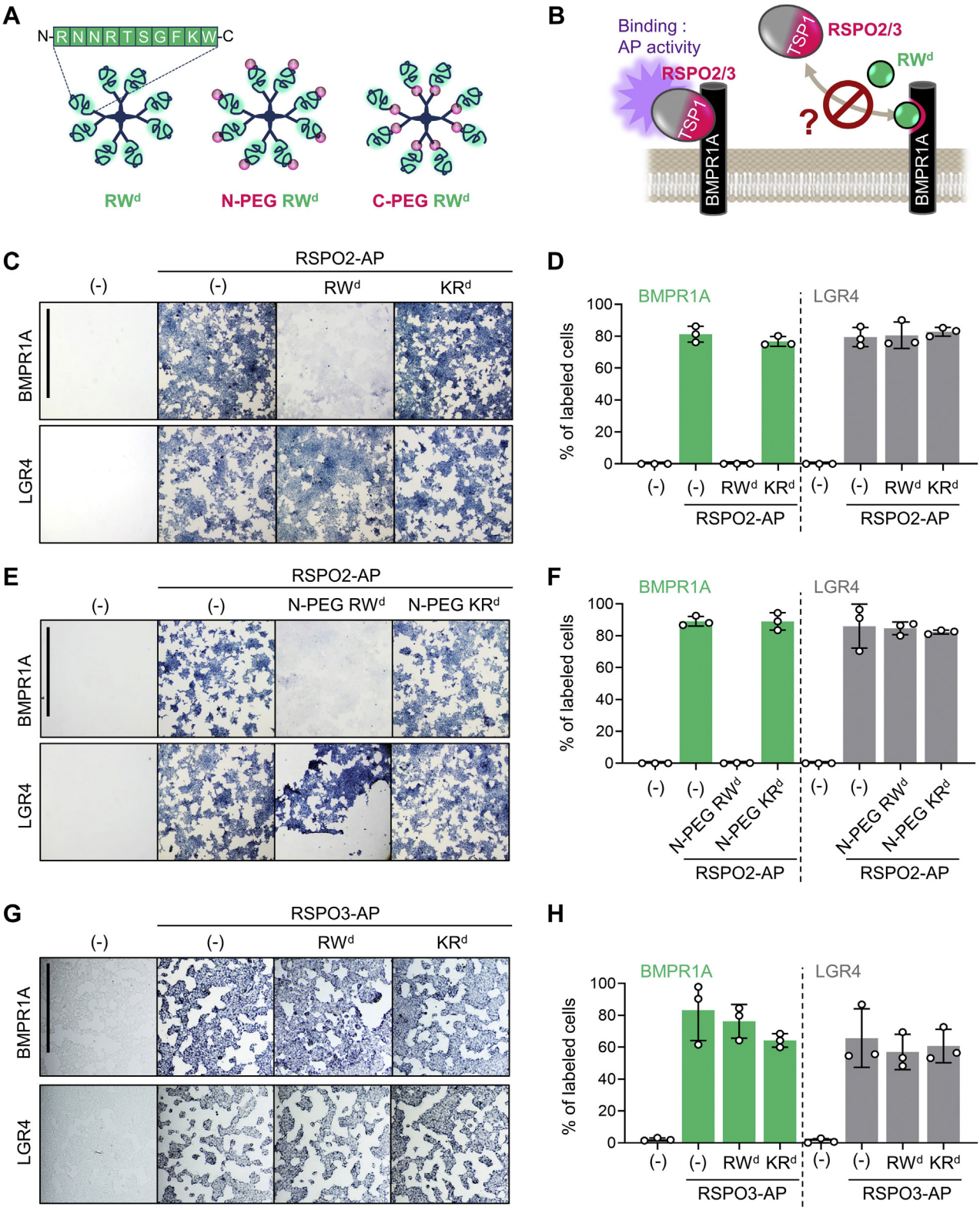

Figure 2. RW dendrimer blocks RSPO2–BMPR1A interaction at the cell membrane. *A*, cartoons illustrating three different RW dendrimers used in the study. *B*, scheme for cell surface–binding assay in (*C–H*). Cells were transfected with BMPR1A or LGR4 DNA and treated with RSPO2/3-AP with or without 20 μM dendrimers for 3 h as indicated. Binding was detected as *purple stain* on cell surface by chromogenic AP assay. *C*, images of cells transfected with DNA and treated with RSPO2-AP and 20 μM non-PEGylated dendrimers as indicated. Data show a representative from three independent experiments. The scale bar represents 1 mm. *D*, quantification of (*C*). n = 3 biologically independent samples. Data are displayed as means ± SD. *E*, images of cells transfected with DNA and treated with RSPO2-AP and 20 μM N-PEGylated dendrimers as indicated. Data show a representative from three independent experiments. The scale bar represents 1 mm. *F*, quantification of (*E*). n = 3 biologically independent samples. Data are displayed as means ± SD. *G*, images of cells transfected with DNA and treated with RSPO3-AP and 20 μM non-PEGylated dendrimers as indicated. Data show a representative from three independent experiments. The scale bar represents 0.5 mm. *H*, quantification of (*G*). n = 3 biologically independent samples. Data are displayed as means ± SD. AP, alkaline phosphatase; BMPR1A, BMP receptor type 1A; LGR4, leucine-rich repeat containing G protein–coupled receptor 4; PEG, PEGylation; RSPO2, R-spondin 2.

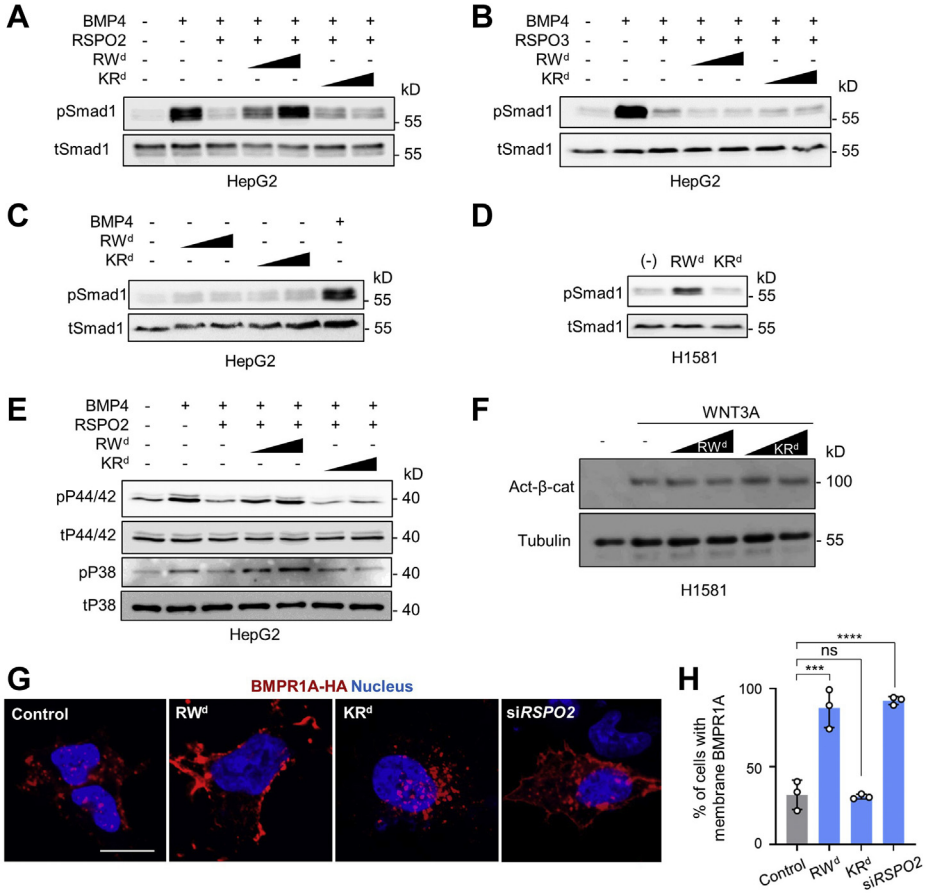

Figure 3. RW dendrimer augments BMP4–BMPR1A signaling. *A*, Western blot analysis of phosphorylated Smad1 (pSmad1) and total Smad1 (tSmad1) in HEPG2 cells stimulated by BMP4, treated with or without RSPO2 and 0.5 μM dendrimers for 1 h as indicated. Cells were starved 3 h before the stimulation. *B*, Western blot analysis of pSmad1 and tSmad1 in HEPG2 cells stimulated by BMP4, treated with or without RSPO3 and 0.5 μM dendrimers for 1 h as indicated. Cells were starved 3 h before the stimulation. *C*, Western blot analysis of pSmad1 and tSmad1 in HEPG2 cells treated with or without 0.5 μM dendrimers for 3 days as indicated. BMP4 was treated as a control. Cells were starved 6 h before the stimulation. *D*, Western blot analysis of pSmad1 and tSmad1 in H1581 cells treated with or without 0.5 μM dendrimers for 3 days as indicated. *E*, Western blot analysis of phosphorylated P38 (pP38), phosphorylated P44/42 (pP44/42), total P38 (tP38), and total P44/42 (tP44/42) MAP kinases in HEPG2 cells stimulated by BMP4, treated with or without RSPO2 and 0.5 μM dendrimers for 1 h as indicated. Cells were starved overnight before the stimulation. *F*, Western blot analysis of activated β-catenin in H1581 cells treated with WNT3A and 0.5 μM dendrimers as indicated. Tubulin was used as a control. *G*, immunofluorescence in H1581 cells transfected with BMPR1A-HA upon 0.5 μM RW and KR dendrimer treatment or si*RSPO2* treatment for 3 days. BMPR1A (*red*) was stained against HA antibody. The scale bar represents 20 μm. *H*, quantification of cells harboring membrane-localized BMPR1A from (*G*). BMP4, bone morphogenetic protein 4; BMPR1A, BMP receptor type 1A; HA, hemagglutinin; HEPG2, human hepatocellular carcinoma cell line; MAP, mitogen-activated protein; RSPO2, R-spondin 2; Smad, small mothers against decapentaplegic.

pP44/42 levels (Fig. 3*E*), confirming that RW^d diminishes the BMP antagonist function of RSPO2.

In contrast to both Smad1 and non-Smad1 BMP signaling, RW^d had no effect on WNT-mediated activation of β-catenin (Fig. 3*F*), corroborating that RW modulates BMP signaling specifically and confirming that the dual function of RSPO2 in BMP and WNT signaling can be uncoupled.

Since RSPO2 antagonizes BMP4 signaling by inducing membrane clearance of BMPR1A (14), we hypothesized that RW^d stabilizes BMPR1A at the plasma membrane. We monitored localization of overexpressed BMPR1A (BMPR1A-HA) by immunofluorescence and found indeed upon RW^d but not KR^d treatment an increase (approximately threefold) in the number of cells showing BMPR1A-HA membrane staining, similar to siRNA knockdown of *RSPO2* (Fig. 3, *G* and *H*), consistent with our model of RW blocking the RSPO2–BMPR1A interaction (Fig. 1*A*). Collectively, we conclude that RW^d derepresses BMP4–BMPR1A signaling by specifically neutralizing RSPO2 as a BMPR1A antagonist.

RW dendrimer induces THP-1 differentiation and inhibits cell growth

We recently showed that RSPO2 inhibits BMP signaling in AML cells to maintain self-renewal and prevent differentiation independent of WNT signaling (26). We therefore asked whether RW^d could reduce endogenous RSPO2 activity of THP-1 AML cells to upregulate BMP signaling and thereby induce monocyte to macrophage ($CD11B^+$) differentiation. Such an effect would mimic cell differentiation therapy of leukemic cells. Indeed, RW^d but not KR^d treatment induced pSmad1 (Fig. 4, *A*–*C*). Elevated pSmad1 levels were detected in nonmodified-treated cells, N-PEG-treated cells, and C-PEG RW^d-treated cells, suggesting that PEGylation does not

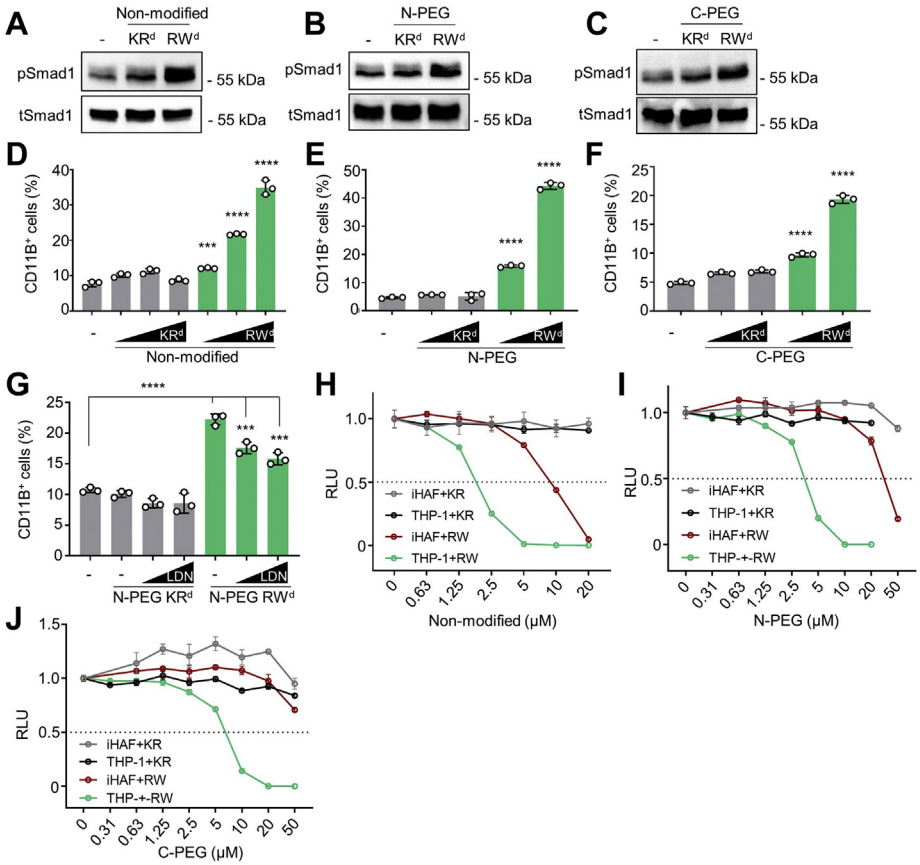

Figure 4. RW dendrimers induce THP-1 differentiation and growth inhibition. *A–C*, Western blot analysis of phosphorylated Smad1 (pSmad1) and total Smad1 (tSmad1) in THP-1 cells stimulated by dendrimers for 3 days as indicated. *A*, cells were treated with 0.5 μM nonmodified dendrimer. *B*, cells were treated with 0.5 μM N-PEG dendrimer. *C*, cells were treated with 2.0 μM C-PEG dendrimer. *D–F*, quantification of $CD11B^+$ THP-1 cells in the flow cytometry analysis. *D*, cells were treated with 0.5/1.0/1.5 μM nonmodified dendrimer for 3 days (*E*), cells were treated with 2.0/3.0 μM N-PEG dendrimer for 3 days (*F*), and cells were treated with 3.0/4.0 μM C-PEG dendrimer for 3 days. $CD11B^-$ cells were defined by the staining of isotype-matched control antibody. *G*, quantification of $CD11B^+$ THP-1 cells in the flow cytometry analysis. Cells were treated with 2.0 μM N-PEG dendrimer for 3 days. After costimulation with 0.5/1.0 μM LDN-193189 for 24 h, cells were harvested for a flow cytometry analysis. *H–J*, cell viability assay of THP-1 and iHAF cells upon dendrimer treatment. THP-1 and iHAF cells were incubated with increasing amounts of dendrimers for 48 h. Cell viability was measured with a luminescent-based assay. iHAF, immortalized human adult fibroblast cell line; RLU, relative light unit; Smad, small mothers against decapentaplegic.

interfere with the functionality of RW^d. Moreover, Dox-inducible sh*RSPO2* knockdown abolished the ability of RW^d to induce pSMAD1, supporting that RW^d functions *via* RSPO2 (Fig. S3, *A* and *B*). Importantly, by flow cytometric analysis, RW^d treatment induced the number of $CD11B^+$ cells up to ∼10-fold, indicating effective monocyte to macrophage differentiation (Fig. 4, *D–F*). Consistently, treatment with BMPR inhibitor LDN-193189 reverted induction of $CD11B^+$ cell by RW^d (Fig. 4*G*).

To confirm that RW^d increases BMP signaling and induces THP-1 differentiation independently of WNT signaling, we stimulated THP-1 cells with WNT3A, analyzed active β-catenin levels, and found them unaffected by RW^d treatment (Fig. S3, *C* and *D*). We conclude that RW^d specifically relieves BMP inhibition by RSPO2 in THP-1 cells and thereby induces their monocyte to macrophage differentiation.

In AML, RSPO2 acts as autocrine growth factor to maintain self-renewal and cell proliferation (26). Hence, inhibition of RSPO2 by RW^d may provide a therapeutic benefit in AML, by derepressing BMP signaling and reducing cancer cell viability. Consistently, RW^d efficiently reduced viability of THP-1 cells in a dose-dependent manner, with the IC_{50} of 1.8, 3.6, and 6.5 μM for nonmodified dendrimer, N-PEG dendrimer, and C-PEG dendrimer, respectively (Fig. 4, *H–J*). In contrast, immortalized human adult fibroblasts cell line (iHAFs) as control cells were less affected by RW^d, tolerating 10-fold higher dendrimer treatment. Moreover, unlike RW^d, KR^d did not affect the viability of either THP-1 or iHAF cells. The results raise the possibility of a therapeutic window of higher sensitivity in AML cells to $RSPO2^{BMP}$ inhibition.

RW dendrimer increases BMP signaling in Xenopus *embryonic axis development*

To analyze the efficacy and specificity of RW^d *in vivo*, we employed *Xenopus* embryos, where an activity gradient of BMP signaling regulates dorsoventral axis formation (42–44), and *Rspo2* acts as negative feedback regulator (14). The RW peptide sequence is completely conserved between human and *Xenopus* (Fig. 5*A*), suggesting that administration of RW^d might impact *Xenopus* dorsoventral axis formation by upregulating BMP signaling. *bmp4* overexpression characteristically induces

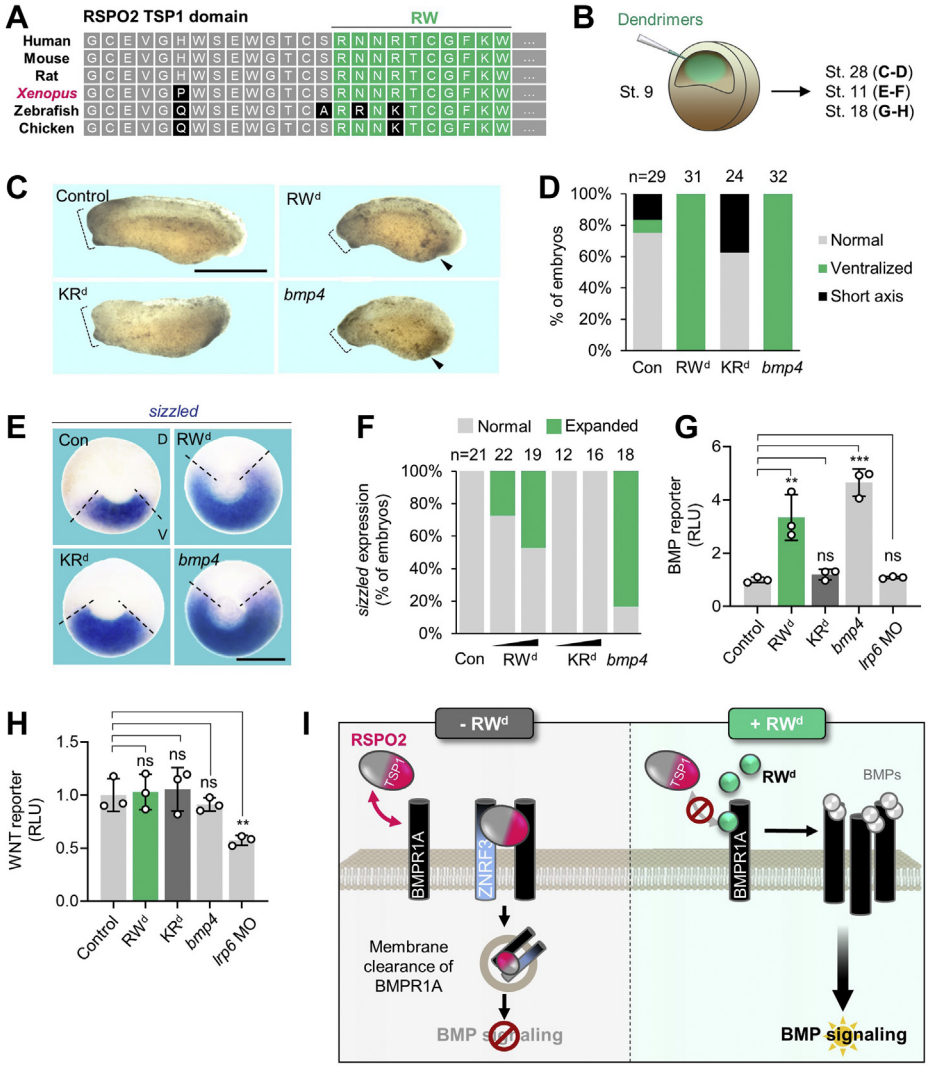

Figure 5. RW dendrimer increases BMP signaling during *Xenopus* embryogenesis independently of WNT signaling. *A*, amino acid sequence comparison of RSPO2 TSP1 domain in human, mouse, and *Xenopus*. Note that RW peptide sequence derived from human RSPO2 is highly conserved among species (*green boxes*). *B*, microinjection strategy for (*C–H*). Emulsion of RW^d or KR^d was injected into the blastocoel of stage 9 *Xenopus tropicalis* embryos and cultured until tailbud (stage 28) (*C* and *D*) or harvested at gastrulae and neurulae (stage 11; *E* and *F*; stage 18, *G* and *H*). *bmp4* mRNA was injected radially at four-cell stage embryos as a control. *C*, representative phenotypes of *Xenopus tropicalis* tailbud (stage 28) injected as indicated. *Dashed lines*, head size. *Arrowheads*, enlarged ventral structure. Note that RW^d-injected tailbud phenocopies *bmp4* overexpressed tailbud. The scale bar represents 1 mm. *D*, quantification of embryonic phenotypes shown in (*C*). "Ventralized" represents embryos with both small head and enlarged ventral structure, reminiscent of BMP hyperactivation. "Short axis" refers to embryos with shorter body length, unrelated to BMP signaling. n = number of embryos. *E*, *in situ* hybridization of *sizzled* in *Xenopus* gastrulae (stage 11, dorsal to the top, *vegetal view*) injected as indicated. *Dashed line*, *sizzled* expressing area. The scale bar represents 0.5 mm. *F*, quantification of *sizzled* expression shown in (*E*). Data are pooled from two independent experiments. n = number of embryos. *G* and *H*, BMP-(*vent2*) reporter assay (*G*) and WNT-(*TOPFlash*) reporter assay (*H*) with *Xenopus tropicalis* neurulae (stage 18) injected with reporter plasmids at stage 3 and then injected with dendrimers at stage 9 as indicated or simultaneously injected with *bmp4* mRNA or *lrp6* morpholino (MO). Data are biological replicates. n = biologically independent samples and data are displayed as means ± SD, with unpaired *t* test. ns, not significant. $^{**}p < 0.01$, $^{****}p < 0.0001$ from two-tailed unpaired *t* test. *I*, model showing the mode of action for RW^d to intervene RSPO2–BMPR1A and modulate BMP signaling. BMP, bone morphogenetic protein; BMPR1A, BMP receptor type 1A; D, dorsal; RSPO2, R-spondin 2; RW^d, RW dendrimer; TSP1, thrombospondin 1; V, ventral.

ventralized embryos, featuring small heads and enlarged ventral structures (Fig. 5, *C* and *D*) (14). Hence, we injected RW^d or KR^d into the blastocoel cavity of *Xenopus* blastulae (Fig. 5*B*). Interestingly, injection of RW^d, but not KR^d, closely phenocopied *bmp4* overexpression (Fig. 5, *C* and *D*) and expanded BMP target gene expression (*sizzled*) toward the dorsal side (Fig. 5, *E* and *F*) indicative of ventralization. Of note, both dendrimers induced only a minor growth retardation during gastrulation that may be due to blastocoel swelling after injection but showed no embryotoxicity. To confirm that RW^d-mediated defects were due to upregulated BMP signaling but not reduced WNT signaling, we performed BMP-responsive *Vent2* reporter assays (Fig. 5*G*) and WNT-responsive TopFlash reporter assays (Fig. 5*H*) using RW^d injected embryos or KR^d injected embryos. While RW^d expectedly enhanced endogenous BMP signaling (Fig. 5*G*), it had no effect on WNT signaling, unlike antisense morpholino inhibition of the WNT receptor Lrp6 (Fig. 5*H*). The results indicate that RW^d is stable *in vivo* and hyperactivates endogenous BMP signaling independently of WNT signaling.

Discussion

The dual function of RSPO2 as BMP antagonist and WNT agonist raises important questions about its mode of action in the many biological processes where RSPO2 is implicated, ranging from development to cancer (14, 18, 21, 26, 31, 45–48). Our study provides an important step toward addressing these questions by corroborating RSPO2 as BMP receptor antagonist and providing a proof of concept and a research tool for pharmacologically uncoupling BMP antagonist from WNT agonist function of RSPO2 with the inhibitor RW^d.

Uncoupling BMP antagonist from WNT agonist function of RSPO2 with the inhibitor RW^d

Building on the fact that RSPOs binds BMPR1A specifically *via* its TSP1 domain (11), we identified a TSP1-derived 10-mer peptide "RW" and improved its efficacy in a dendrimer, which competes for binding of RSPO2 to BMPR1A. RSPOs consist of FU1, FU2, and TSP1 domains. While both the FU1 domain and the TSP1 domain of RSPO2 are important to destabilize cell surface BMPR1A (14), utilizing a FU1 domain–derived peptide to target BMPR1A signaling would be inadequate since the FU1 domain engages the E3 ubiquitin ligase ZNRF3/RNF43 that is also crucial to potentiate WNT signaling. Instead, we took advantage of the specificity of the TSP1 domain for antagonizing BMP4 signaling, which is dispensable for WNT signaling (14). We confirmed that RW^d neither affects LGR4 binding nor impairs WNT/β-catenin signaling in H1581 and THP-1 cells or *Xenopus* embryos.

RW directly binds to the BMPR1A extracellular domain and likely does so at the RSPO2 interaction site in BMPR1A, which is unknown, though. Hence, RW^d presumably functions as a BMPR1A binder that prevents RSPO2 docking. RW^d binding to BMPR1A does not change BMP signaling directly, since in the absence of RSPO2, as in HEPG2 cells or in sh*RSPO2*-treated THP-1 cells, the dendrimer does not affect BMP signaling (Figs. 3*B* and S3*B*). Consistent with the mode of action whereby a RSPO2–ZNRF3 complex ultimately internalizes BMPR1A (11), RW^d counteracts BMPR1A internalization and stabilizes the receptor at the plasma membrane (Fig. 3, *G* and *H*). Our previous study showed that RSPO3 can also inhibit BMP signaling, and it likely does so by a similar mechanism (14). It is therefore surprising that RW^d does not also prevent RSPO3 from BMP signaling inhibition (Fig. 3*B*), suggesting that the slight amino acid differences between the RSPO2 and RSPO3 TSP1 domains manifest in distinct binding modes that can be discerned with a competitor peptide.

Altogether, the results corroborate RSPO2-mediated inhibition of BMP4–BMPR1A signaling by showing that RW^d functions as competitor against RSPO2 to access BMPR1A, stabilizes BMPR1A at the plasma membrane, and promotes BMP4 signaling (Fig. 5*I*). Moreover, they demonstrate pharmacological uncoupling of BMP antagonist from WNT agonist function of RSPO2 with the inhibitor RW^d.

Projecting from the RW^d approach, it may be possible to specifically interfere with RSPO2/LGR/WNT signaling *via* dendrimer analogs of FU2, the domain that engages LGR4/5/6 but that is not required for antagonizing BMP signaling (11). Along similar lines, RSPO mutants were recently described to target LGRs (49, 50).

Targeting RSPO2–BMPR1A interaction by RW^d as a potential therapeutic approach for AML

AML is an aggressive disease with rapid progression of undifferentiated myeloid blasts, and there is the need of additional therapeutic targets and reagents (51, 52). RSPOs, in particular RSPO2 and RSPO3, maintain the growth and differentiation—block of AML cells and high RSPO2 expression correlate with adverse disease status (26, 48). By targeting BMPR1A, autocrine RSPO2 acts as a BMP antagonist to promote AML stem cell self-renewal, and loss of RSPO2 delays AML progression (26). Phenocopying RSPO2 deficiency in THP-1 cells (26), RW^d disrupts the interaction between RSPO2 and BMPR1A, increases BMP signaling, inhibits cell growth, and induces monocyte to macrophage differentiation. These observations not only corroborate the relevance of RSPO2 in AML but also suggest that harnessing the RSPO2–BMPR1A interaction may be beneficial in AML therapy.

A number of studies have identified BMP2 and BMP7-mimetic peptides that globally augment BMP signaling (53–58). These mimetics typically show strong affinity to BMPRs and activate signaling ligand independently. Given the many roles of BMP signaling in normal cell homeostasis, administration of these mimetics may result in severe side effects (59). In contrast, RW^d specifically impairs the RSPO2–BMPR1A interaction, restricting upregulated BMP signaling to cells where BMPR1A is predominant in transmitting BMP signaling and is subject to RSPO inhibition. This specificity limits on the one hand the applicability of a therapeutic approach to fewer cell lineages; on the other hand, it avoids generalized BMP signaling upregulation and reduces potential side effects.

Modulating protein–protein interaction by inhibitory peptides attracts increasing attention since they may target protein–protein interactions with high specificity and affinity. However, peptide-based reagents frequently suffer from poor pharmacokinetics because of their short half-life (60–62). Emerging strategies enhance the stability of therapeutic peptides by introducing chemical modifications, assembling monomers into highly ordered complexes, or by designing for peptide analogs (63). Different from RW monomer, which has poor *in vivo* inhibitory function on RSPO2–BMPR1A, RW dendrimer features enhanced peptide stability and avidity and robustly inhibits RSPO2 in the micromolar range. A large therapeutic window is a key criterion for drug development as it limits potential side effects in normal cell (64). We observed no *Xenopus* embryotoxicity of RW^d at concentrations that robustly induced BMP signaling, and human adult fibroblasts tolerate at least 10-fold higher RW^d concentrations than THP-1 cells. However, therapeutic application requires a reagent of higher affinity than that of RW^d, which acts in the micromolar range. Computational modeling and medicinal chemistry may

derive small molecules mimicking RW^{d} with improved pharmacological properties.

Looking beyond AML, RSPO2 is implicated in various other cancer entities, notably colon cancer (45, 46, 48, 65). The availability of RW^{d} invites to explore both the potential role and therapeutic opportunities of RSPO–BMP inhibition in these contexts in the future.

Experimental procedures

Synthetic peptides

All peptides used in the study were synthesized and obtained from ProteoGenix, Inc. For overlapping peptide screening, monomeric peptides derived from the TSP1 domain of human RSPO2 (14) were designed with exchange of internal Cys to Ser residue. Peptides were synthesized and obtained of >70% purity, without modifications. Lyophilized peptides were reconstituted in Dulbecco's PBS (DPBS), adjusted with pH 7.4 (GW, HR, GC, RW, GV, TK, KC, DE, PK, and SG) or in DPBS with 0.1% dimethyl sulfoxide, adjusted with pH 7.4 (CR). For PEGylated monomeric peptide, RW and TK peptides were mini-PEGylated at both N and C termini and reconstituted in DPBS, pH 7.4. For dendrimerized RW and KR, individual peptides were synthesized and assembled on an octavalent Lys core matrix, forming an 8-mer complex with purity of >80%. The sequences for the RW and KR dendrimers are (RNNRTSGFKW)8-Lys4-Lys2-Lys-β-Ala (RW dendrimer) and (KMTMR)8-Lys4-Lys2-Lys-β-Ala (KR dendrimer), respectively. For PEGylated dendrimers, mini-PEGylation of individual peptides within the dendrimers was performed at the N- or C-terminus, followed by attachment to the core matrix (designated as N-PEG dendrimer or C-PEG dendrimer, respectively). The sequences of N- and C-PEG RW dendrimers are (PEG-RNNRTSGFKW)8-Lys4-Lys2-Lys-β-Ala and (RNNRTSGFKW-PEG)8-Lys4-Lys2-Lys-β-Ala. The sequences of N- and C-PEG KR dendrimers are (PEG-KMTMR)8-Lys4-Lys2-Lys-β-Ala and (KMTMR-PEG)8-Lys4-Lys2-Lys-β-Ala. The type of dendrimer used for each experiment is indicated in the figure legends. For biotinylated RW and TK peptides, peptides were synthesized and terminally modified by the addition of Biotin with a 6-aminohexanoic acid or ethylenediamine spacer at the N- or C-terminus, respectively.

Cell lines and growth conditions

Human embryonic kidney 293T cells (HEK293T) and HEPG2 cells (American Type Culture Collection) were maintained in Dulbecco's modified Eagle's medium-high glucose (catalog no.: 11960; Gibco) with 10% fetal bovine serum (FBS) (catalog no.: FBS-12A; Capricorn), 1% penicillin–streptomycin (catalog no.: P0781; Sigma), and 2 mM L-glutamine (catalog no.: G7513; Sigma). H1581 cells (gift from Dr R. Thomas) were maintained in RPMI (catalog no.: 21875; Gibco) with 10% FBS, 1% penicillin–streptomycin, 2 mM L-glutamine, and 1 mM sodium pyruvate (catalog no.: S8636; Sigma). THP-1 cells were maintained in RPMI with 10% FBS, 1% penicillin–streptomycin, 2 mM L-glutamine, and 1 mM sodium pyruvate. iHAFs were derived from primary human adult fibroblasts immortalized using large T antigen and kindly provided by Prof Jochen S. Utikal, DKFZ. All cell lines were cultured at 37 °C and 5% CO_2 in a humidity-controlled incubator. Mycoplasma contamination was negative in all cell lines used.

Production of conditioned medium

Conditioned medium was generated as previously described (14). In brief, HEK293T cells were seeded in 10 or 15 cm culture dishes and transiently transfected with RSPO2-AP, RSPO3-AP, RSPO2^{TSP1}-HA, or BMPR1A^{ECD}-AP plasmids, followed by harvesting three times every 2 days. Produced medium was validated with Western blot analyses and AP activity analyses.

In vitro *competitive binding assay*

High-binding 96-well plates (catalog no.: M5811; Greiner) were coated with 1 to 2 μg of anti-HA antibody (catalog no.: 11867423001; Roche) overnight at 4 °C. Coated wells were blocked with 5% bovine serum albumin in TBS with Tween-20 (TBST) for 1 h, followed by washing with TBST. Wells were treated overnight with HA-tagged RSPO2^{TSP1} conditioned media, followed by treatment of AP-tagged BMPR1A^{ECD} in combination with 100 μM of monomeric peptides or with increasing concentration of monomeric RW peptide for 3 h. Wells were washed with TBST, and bound AP activity was measured by the chemiluminescent AquaSpark AP substrate (catalog no.: 42593.01; Serva). Validation of IC_{50} was executed using GraphPad (GraphPad Software, Inc).

In vitro *direct binding assay*

Streptavidin-coated 96-well plates (catalog no.: 15218; Thermo Fisher Scientific) were incubated with biotinylated RW and TK peptides (50 μM) for 3 h, followed by washing with TBST. Wells were treated overnight with AP-tagged BMPR1A^{ECD}. Wells were washed with TBST, and bound AP activity was measured by the chemiluminescent AquaSpark AP substrate (catalog no.: 42593.01; Serva).

Cell surface–binding assay

Cell surface–binding assays were executed as previously described (14). In brief, HEK293T cells were transfected with BMPR1A-HA and LGR4 DNA and incubated with conditioned media in combination with 50 μM monomeric peptides or 20 μM dendrimers for 3 h or 16 h. Surface binding was detected by development with BM-Purple (catalog no.: 11442074001; Sigma). Images were obtained with DMIL microscope/Canon DS126311 camera (LEICA).

Western blot analysis

Cultured HEPG2, H1581, and THP-1 cells were lysed in Triton lysis buffer (14) or radioimmunoprecipitation buffer with cOmplete Protease Inhibitor Cocktail (catalog no.: 11697498001; Roche). SDS-PAGE samples were prepared with lysates mixed with Laemmli buffer containing β-mercaptoethanol, followed by boiling at 95 °C for 5 min. Western blot

images were acquired with SuperSignal West pico ECL (catalog no.: 34580; Thermo Fisher Scientific) or Clarity Western ECL (catalog no.: 1705061; Bio-Rad) using LAS-3000 system (FujiFilm).

Immunofluorescence

H1581 cells were transfected with BMPR1A-HA using Lipofectamine 3000 (catalog no.: L3000; Invitrogen). After 48 h, cells were treated with 0.5 μM RW or KR dendrimers and fixed in 4% paraformaldehyde for 10 min. Cells were treated with primary antibodies (1:250) overnight at 4 °C, and secondary antibodies (1:500) and Hoechst dye (1:500) were applied for 2 h at room temperature. Images were obtained using an LSM 700 microscope (Zeiss). Quantification was executed using ImageJ, version 1.51k software (https://imagej.nih.gov/ij/).

Fluorescence-activated cell sorting analysis

For the differentiation analysis of THP-1, cells were harvested, pelleted, and resuspended in ice-cold blocking buffer (PBS supplemented with 1% bovine serum albumin and 0.1% NaN_3). Cells were treated with Fc receptor binding inhibitor as recommended by the manufacturer (catalog no.: 14916173; eBioscience) and stained directly with FITC-conjugated antibodies diluted in blocking buffer. Isotype-matched antibodies were used as control. Dead cells were excluded by counterstaining with propidium iodide. Samples were analyzed with FACSCanto (fluorescence-activated cell sorting (FACS); BD Biosciences). About 10,000 events per samples were acquired, and results were processed with FACSDiva software (BD Biosciences) or FlowJo (FlowJo, LLC).

Cell viability assay

Cells were seeded into 96-well plate in high density with increasing amounts of dendrimers. After incubation of 48 h, cells were harvested, and viability was measured with a CellTiter-Glo Luminescent Cell Viability Assay kit (catalog no.: G7570; Promega) according to the manufacturer's instructions.

Xenopus *tropicalis*

Xenopus tropicalis male and female frogs were obtained from Nasco, National *Xenopus* Resource and European *Xenopus* Resource Centre. All *X. tropicalis* experiments were approved by the state review board of Baden–Württemberg, Germany (permit number: G-141-18) and executed according to federal and institutional guidelines and regulations. Developmental stages of the embryos were determined according to Nieuwkoop and Faber (Xenbase; https://www.xenbase.org).

Xenopus *microinjection*

In vitro fertilization, microinjection, and culture of *X. tropicalis* embryos were executed following the protocol from Xenbase (https://www.xenbase.org). *X. tropicalis* embryos were microinjected using Harvard Apparatus microinjection system. About 20 nl of 50 μM reconstituted dendrimers in PBS were microinjected into the blastocoel of stage 9 embryos. Microinjected embryos were cultured until desired stages. For phenotype analysis, scoring of phenotypes was executed with blinding, and data are representative images from two independent experiments. *Xenopus* images were obtained using AxioCam MRc 5 microscope (Zeiss). Embryos in each image were selected using Magnetic Lasso tool or Magic Wand tool of Adobe Photoshop CS6 software and pasted into the uniform background color for presentation.

X. tropicalis *whole-mount* in situ *hybridization*

Whole-mount *in situ* hybridizations of *X. tropicalis* embryos were performed using digoxigenin-labeled probes according to the standard protocol (https://www.xenbase.org) (66). Antisense RNA probes against *sizzled* was synthesized as previously described (14). Representative images were obtained using AxioCam MRc 5 microscope. Embryos in each image were selected using Magnetic Lasso tool or Magic Wand tool of Adobe Photoshop CS6 software and pasted into the uniform background color for presentation.

Xenopus *reporter assays*

Xenopus embryos were microinjected with 200 pg of *Vent-Luc* or *Topflash* along with 100 pg of *Renilla-TK* plasmid DNA at 2-cell stage. At stage 9, 20 nl of 50 μM reconstituted dendrimers in PBS was microinjected into the blastocoel of embryos. Three pools of four embryos each at stage 14 to 15 were lysed with passive lysis buffer, and luciferase activity was measured with the dual luciferase reporter assay system (catalog no.: E1960; Promega). Firefly luminescence (Vent2/TopFlash) was normalized to Renilla. Data are displayed as average of biological replicates with SD. Statistical analyses were made with the PRISM7 software (GraphPad Software, Inc) using unpaired *t* test or one-way ANOVA test. Not significant (ns) $^{**}p < 0.01$ and $^{***}p < 0.001$.

Antibodies

Phospho-Smad1/5 (Ser463/465) (catalog no.: 9516; Cell Signaling), Smad1 (catalog no.: 9743; Cell Signaling), active-β-catenin (catalog no.: 05-665; Millipore), α-tubulin (catalog no.: T5168; Sigma), HA (catalog no.: 11867423001; Roche), donkey anti-rat (Alexa 488) (catalog no.: A-21208; Thermo), CD11B (catalog no.: 557396; BD Biosciences), phospho-P38 MAPK (T180/Ty182) (catalog no.: 9211; Cell Signaling), phospho-P44/42 MAPK (catalog no.: 9101; Cell Signaling), P38 MAPK (catalog no.: 9212; Cell Signaling), and P44/42 MAPK (catalog no.: M5670; Sigma).

Data availability

All raw data are available upon reasonable request.

Supporting information—This article contains supporting information.

Acknowledgments—We acknowledge Dr G. Roth and Aska Pharmaceuticals Tokyo for generously providing human chorionic

gonadotropin. We thank National *Xenopus* Resource (Research Resource Identifier: SCR_013731), Xenbase (Research Resource Identifier: SCR_004337), and European *Xenopus* Resource Centre for *Xenopus* resources. We thank Dr Andrey Glinka for critical discussion of the article. Expert technical support by the DKFZ core facility for light microscopy and the central animal laboratory of DKFZ is gratefully acknowledged.

Author contributions—H. L., R. S., and C. N. conceptualization; H. L. and R. S. methodology; H. L. and R. S. formal analysis; H. L. and R. S. investigation; H. L., R. S., and C. N. writing–original draft; H. L., R. S., and C. N. writing–review & editing; C. N. supervision; C. N. funding acquisition.

Funding and additional information—This work was funded by the Deutsche Forschungsgemeinschaft (German Research Foundation) to C. N. (grant no.: SFB1324-B01).

Conflict of interest—The authors declare that they have no conflicts of interest with the contents of this article.

Abbreviations—The abbreviations used are: ACVR1, activin A receptor type I; AML, acute myeloid leukemia; AP, alkaline phosphatase; BMP, bone morphogenetic protein; BMPR1A, BMP receptor type 1A; DPBS, Dulbecco's PBS; ECD, extracellular domain; FBS, fetal bovine serum; FU, furin-like repeat; HA, hemagglutinin; HEK293T, human embryonic kidney 293T cell line; HEPG2, human hepatocellular carcinoma cell line; iHAF, immortalized human adult fibroblast cell line; LGR, leucine-rich repeat containing G protein–coupled receptor; LRP, lipoprotein receptor–related protein; MAP, mitogen-activated protein; MAPK, mitogen-activated protein kinase; pSmad1, Smad1 phosphorylation; RNF43, ring finger 43; RSPO2, R-spondin 2; $RSPO2^{TSP1}$, TSP1 domain of RSPO2; RW^{d}, RW dendrimer; SMAD, small mothers against decapentaplegic; TBST, TBS with Tween-20; TSP1, thrombospondin 1; ZNRF3, zinc and ring finger 3.

References

1. David, C. J., and Massague, J. (2018) Contextual determinants of TGFbeta action in development, immunity and cancer. *Nat. Rev. Mol. Cell Biol.* **19**, 419–435
2. Salazar, V. S., Gamer, L. W., and Rosen, V. (2016) BMP signalling in skeletal development, disease and repair. *Nat. Rev. Endocrinol.* **12**, 203–221
3. Zhang, Y., and Que, J. (2020) BMP signaling in development, stem cells, and diseases of the gastrointestinal tract. *Annu. Rev. Physiol.* **82**, 251–273
4. Zylbersztejn, F., Flores-Violante, M., Voeltzel, T., Nicolini, F. E., Lefort, S., and Maguer-Satta, V. (2018) The BMP pathway: A unique tool to decode the origin and progression of leukemia. *Exp. Hematol.* **61**, 36–44
5. Wu, M., Chen, G., and Li, Y. P. (2016) TGF-beta and BMP signaling in osteoblast, skeletal development, and bone formation, homeostasis and disease. *Bone Res.* **4**, 16009
6. Lowery, J. W., Brookshire, B., and Rosen, V. (2016) A survey of strategies to modulate the bone morphogenetic protein signaling pathway: Current and future perspectives. *Stem Cells Int.* **2016**, 7290686
7. Heldin, C. H., and Moustakas, A. (2016) Signaling receptors for TGF-beta family members. *Cold Spring Harb. Perspect. Biol.* **8**, a022053
8. Antebi, Y. E., Linton, J. M., Klumpe, H., Bintu, B., Gong, M., Su, C., McCardell, R., and Elowitz, M. B. (2017) Combinatorial signal perception in the BMP pathway. *Cell* **170**, 1184–1196
9. Massague, J. (1998) TGF-beta signal transduction. *Annu. Rev. Biochem.* **67**, 753–791
10. Heldin, C. H., Miyazono, K., and ten Dijke, P. (1997) TGF-beta signalling from cell membrane to nucleus through SMAD proteins. *Nature* **390**, 465–471
11. Zhang, Y. E. (2009) Non-Smad pathways in TGF-beta signaling. *Cell Res.* **19**, 128–139
12. Cai, J., Pardali, E., Sanchez-Duffhues, G., and ten Dijke, P. (2012) BMP signaling in vascular diseases. *FEBS Lett.* **586**, 1993–2002
13. Chang, C. (2016) Agonists and antagonists of TGF-beta family ligands. *Cold Spring Harb. Perspect. Biol.* **8**, a021923
14. Lee, H., Seidl, C., Sun, R., Glinka, A., and Niehrs, C. (2020) R-spondins are BMP receptor antagonists in Xenopus early embryonic development. *Nat. Commun.* **11**, 5570
15. Chartier, C., Raval, J., Axelrod, F., Bond, C., Cain, J., Dee-Hoskins, C., Ma, S., Fischer, M. M., Shah, J., Wei, J., Ji, M., Lam, A., Stroud, M., Yen, W. C., Yeung, P., *et al.* (2016) Therapeutic targeting of tumor-derived R-spondin attenuates beta-catenin signaling and tumorigenesis in multiple cancer types. *Cancer Res.* **76**, 713–723
16. de Lau, W., Peng, W. C., Gros, P., and Clevers, H. (2014) The R-spondin/Lgr5/Rnf43 module: Regulator of Wnt signal strength. *Genes Dev.* **28**, 305–316
17. Hao, H. X., Jiang, X., and Cong, F. (2016) Control of Wnt receptor turnover by R-spondin-ZNRF3/RNF43 signaling module and its dysregulation in cancer. *Cancers* **8**, 54
18. Kazanskaya, O., Glinka, A., del Barco Barrantes, I., Stannek, P., Niehrs, C., and Wu, W. (2004) R-Spondin2 is a secreted activator of Wnt/beta-catenin signaling and is required for Xenopus myogenesis. *Dev. Cell* **7**, 525–534
19. Kim, K. A., Kakitani, M., Zhao, J., Oshima, T., Tang, T., Binnerts, M., Liu, Y., Boyle, B., Park, E., Emtage, P., Funk, W. D., and Tomizuka, K. (2005) Mitogenic influence of human R-spondin1 on the intestinal epithelium. *Science* **309**, 1256–1259
20. Nanki, K., Toshimitsu, K., Takano, A., Fujii, M., Shimokawa, M., Ohta, Y., Matano, M., Seino, T., Nishikori, S., Ishikawa, K., Kawasaki, K., Togasaki, K., Takahashi, S., Sukawa, Y., Ishida, H., *et al.* (2018) Divergent routes toward Wnt and R-spondin Niche independency during human gastric carcinogenesis. *Cell* **174**, 856–869
21. Seshagiri, S., Stawiski, E. W., Durinck, S., Modrusan, Z., Storm, E. E., Conboy, C. B., Chaudhuri, S., Guan, Y., Janakiraman, V., Jaiswal, B. S., Guillory, J., Ha, C., Dijkgraaf, G. J., Stinson, J., Gnad, F., *et al.* (2012) Recurrent R-spondin fusions in colon cancer. *Nature* **488**, 660–664
22. Carmon, K. S., Gong, X., Lin, Q., Thomas, A., and Liu, Q. (2011) R-spondins function as ligands of the orphan receptors LGR4 and LGR5 to regulate Wnt/beta-catenin signaling. *Proc. Natl. Acad. Sci. U. S. A.* **108**, 11452–11457
23. Glinka, A., Dolde, C., Kirsch, N., Huang, Y. L., Kazanskaya, O., Ingelfinger, D., Boutros, M., Cruciat, C. M., and Niehrs, C. (2011) LGR4 and LGR5 are R-spondin receptors mediating Wnt/beta-catenin and Wnt/PCP signalling. *EMBO Rep.* **12**, 1055–1061
24. Koo, B. K., Spit, M., Jordens, I., Low, T. Y., Stange, D. E., van de Wetering, M., van Es, J. H., Mohammed, S., Heck, A. J., Maurice, M. M., and Clevers, H. (2012) Tumour suppressor RNF43 is a stem-cell E3 ligase that induces endocytosis of Wnt receptors. *Nature* **488**, 665–669
25. Hao, H. X., Xie, Y., Zhang, Y., Charlat, O., Oster, E., Avello, M., Lei, H., Mickanin, C., Liu, D., Ruffner, H., Mao, X., Ma, Q., Zamponi, R., Bouwmeester, T., Finan, P. M., *et al.* (2012) ZNRF3 promotes Wnt receptor turnover in an R-spondin-sensitive manner. *Nature* **485**, 195–200
26. Sun, R., He, L., Lee, H., Glinka, A., Andresen, C., Hubschmann, D., Jeremias, I., Muller-Decker, K., Pabst, C., and Niehrs, C. (2021) RSPO2 inhibits BMP signaling to promote self-renewal in acute myeloid leukemia. *Cell Rep.* **36**, 109559
27. Zebisch, M., Xu, Y., Krastev, C., MacDonald, B. T., Chen, M., Gilbert, R. J., He, X., and Jones, E. Y. (2013) Structural and molecular basis of ZNRF3/RNF43 transmembrane ubiquitin ligase inhibition by the Wnt agonist R-spondin. *Nat. Commun.* **4**, 2787
28. Peng, W. C., de Lau, W., Madoori, P. K., Forneris, F., Granneman, J. C., Clevers, H., and Gros, P. (2013) Structures of Wnt-antagonist ZNRF3 and its complex with R-spondin 1 and implications for signaling. *PLoS One* **8**, e83110

29. Ohkawara, B., Glinka, A., and Niehrs, C. (2011) Rspo3 binds syndecan 4 and induces Wnt/PCP signaling via clathrin-mediated endocytosis to promote morphogenesis. *Dev. Cell* **20**, 303–314
30. Lebensohn, A. M., and Rohatgi, R. (2018) R-spondins can potentiate WNT signaling without LGRs. *Elife* **7**, e33126
31. Szenker-Ravi, E., Altunoglu, U., Leushacke, M., Bosso-Lefevre, C., Khatoo, M., Thi Tran, H., Naert, T., Noelanders, R., Hajamohideen, A., Beneteau, C., de Sousa, S. B., Karaman, B., Latypova, X., Basaran, S., Yucel, E. B., *et al.* (2018) RSPO2 inhibition of RNF43 and ZNRF3 governs limb development independently of LGR4/5/6. *Nature* **557**, 564–569
32. Dubey, R., van Kerkhof, P., Jordens, I., Malinauskas, T., Pusapati, G. V., McKenna, J. K., Li, D., Carette, J. E., Ho, M., Siebold, C., Maurice, M., Lebensohn, A. M., and Rohatgi, R. (2020) R-spondins engage heparan sulfate proteoglycans to potentiate WNT signaling. *Elife* **9**, e54469
33. Craik, D. J., Fairlie, D. P., Liras, S., and Price, D. (2013) The future of peptide-based drugs. *Chem. Biol. Drug Des.* **81**, 136–147
34. Sun, A., Fang, J., and Yan, J. (2013) Advance and development in research of bacterial drug-resistance signaling mechanism and multiple antigenic peptide-based vaccines. *Zhejiang Da Xue Xue Bao Yi Xue Ban* **42**, 125–130
35. Vlieghe, P., Lisowski, V., Martinez, J., and Khrestchatisky, M. (2010) Synthetic therapeutic peptides: Science and market. *Drug Discov. Today* **15**, 40–56
36. Roberts, M. J., Bentley, M. D., and Harris, J. M. (2002) Chemistry for peptide and protein PEGylation. *Adv. Drug Deliv. Rev.* **54**, 459–476
37. Sadler, K., and Tam, J. P. (2002) Peptide dendrimers: Applications and synthesis. *J. Biotechnol.* **90**, 195–229
38. Bracci, L., Falciani, C., Lelli, B., Lozzi, L., Runci, Y., Pini, A., De Montis, M. G., Tagliamonte, A., and Neri, P. (2003) Synthetic peptides in the form of dendrimers become resistant to protease activity. *J. Biol. Chem.* **278**, 46590–46595
39. Liu, J., Gray, W. D., Davis, M. E., and Luo, Y. (2012) Peptide- and saccharide-conjugated dendrimers for targeted drug delivery: A concise review. *Interface Focus* **2**, 307–324
40. Miyazono, K., Kamiya, Y., and Morikawa, M. (2010) Bone morphogenetic protein receptors and signal transduction. *J. Biochem.* **147**, 35–51
41. Zhang, Y. E. (2017) Non-smad signaling pathways of the TGF-beta family. *Cold Spring Harb. Perspect. Biol.* **9**, a022129
42. Harland, R., and Gerhart, J. (1997) Formation and function of Spemann's organizer. *Annu. Rev. Cell Dev. Biol.* **13**, 611–667
43. De Robertis, E. M., Larrain, J., Oelgeschlager, M., and Wessely, O. (2000) The establishment of Spemann's organizer and patterning of the vertebrate embryo. *Nat. Rev. Genet.* **1**, 171–181
44. Niehrs, C. (2004) Regionally specific induction by the Spemann-Mangold organizer. *Nat. Rev. Genet.* **5**, 425–434
45. Zhang, H., Han, X., Wei, B., Fang, J., Hou, X., Lan, T., and Wei, H. (2019) RSPO2 enhances cell invasion and migration via the WNT/beta-catenin pathway in human gastric cancer. *J. Cell Biochem.* **120**, 5813–5824
46. Ilmer, M., Boiles, A. R., Regel, I., Yokoi, K., Michalski, C. W., Wistuba, I. I., Rodriguez, J., Alt, E., and Vykoukal, J. (2015) RSPO2 enhances canonical Wnt signaling to confer stemness-associated traits to susceptible pancreatic cancer cells. *Cancer Res.* **75**, 1883–1896
47. Han, T., Schatoff, E. M., Murphy, C., Zafra, M. P., Wilkinson, J. E., Elemento, O., and Dow, L. E. (2017) R-Spondin chromosome rearrangements drive Wnt-dependent tumour initiation and maintenance in the intestine. *Nat. Commun.* **8**, 15945
48. Salik, B., Yi, H., Hassan, N., Santiappillai, N., Vick, B., Connerty, P., Duly, A., Trahair, T., Woo, A. J., Beck, D., Liu, T., Spiekermann, K., Jeremias, I., Wang, J., Kavallaris, M., *et al.* (2020) Targeting RSPO3-LGR4 signaling for leukemia stem cell eradication in acute myeloid leukemia. *Cancer Cell* **38**, 263–278
49. Cui, J., Toh, Y., Park, S., Yu, W., Tu, J., Wu, L., Li, L., Jacob, J., Pan, S., Carmon, K. S., and Liu, Q. J. (2021) Drug conjugates of antagonistic R-spondin 4 mutant for simultaneous targeting of Leucine-rich repeat-containing G protein-coupled receptors 4/5/6 for cancer treatment. *J. Med. Chem.* **64**, 12572–12581
50. Yu, S., Mulero, M. C., Chen, W., Shang, X., Tian, S., Watanabe, J., Watanabe, A., Vorberg, T., Wong, C., Gately, D., and Howell, S. B. (2021) Therapeutic targeting of tumor cells rich in LGR stem cell receptors. *Bioconjug. Chem.* **32**, 376–384
51. De Kouchkovsky, I., and Abdul-Hay, M. (2016) Acute myeloid leukemia: A comprehensive review and 2016 update. *Blood Cancer J.* **6**, e441
52. Dohner, H., Weisdorf, D. J., and Bloomfield, C. D. (2015) Acute myeloid leukemia. *N. Engl. J. Med.* **373**, 1136–1152
53. Suzuki, Y., Tanihara, M., Suzuki, K., Saitou, A., Sufan, W., and Nishimura, Y. (2000) Alginate hydrogel linked with synthetic oligopeptide derived from BMP-2 allows ectopic osteoinduction *in vivo*. *J. Biomed. Mater. Res.* **50**, 405–409
54. Saito, N., and Takaoka, K. (2003) New synthetic biodegradable polymers as BMP carriers for bone tissue engineering. *Biomaterials* **24**, 2287–2293
55. Li, M., Zhao, Q. H., Chen, Q. X., Liu, M. Z., and Shi, X. W. (2008) Cloning and bioinformatic analysis of bone morphological protein 7 (BMP7) in rabbit. *Yi Chuan* **30**, 885–892
56. Kim, J. E., Lee, E. J., Kim, H. E., Koh, Y. H., and Jang, J. H. (2012) The impact of immobilization of BMP-2 on PDO membrane for bone regeneration. *J. Biomed. Mater. Res. A* **100**, 1488–1493
57. Sugimoto, H., LeBleu, V. S., Bosukonda, D., Keck, P., Taduri, G., Bechtel, W., Okada, H., Carlson, W., Jr., Bey, P., Rusckowski, M., Tampe, B., Tampe, D., Kanasaki, K., Zeisberg, M., and Kalluri, R. (2012) Activin-like kinase 3 is important for kidney regeneration and reversal of fibrosis. *Nat. Med.* **18**, 396–404
58. Tong, Z., Guo, J., Glen, R. C., Morrell, N. W., and Li, W. (2019) A bone morphogenetic protein (BMP)-derived peptide based on the type I receptor-binding site modifies cell-type dependent BMP signalling. *Sci. Rep.* **9**, 13446
59. Shimer, A. L., Oner, F. C., and Vaccaro, A. R. (2009) Spinal reconstruction and bone morphogenetic proteins: Open questions. *Injury* **40**, S32–S38
60. Lu, H., Zhou, Q., He, J., Jiang, Z., Peng, C., Tong, R., and Shi, J. (2020) Recent advances in the development of protein-protein interactions modulators: Mechanisms and clinical trials. *Signal Transduct. Target. Ther.* **5**, 213
61. de Vega, M. J., Martin-Martinez, M., and Gonzalez-Muniz, R. (2007) Modulation of protein-protein interactions by stabilizing/mimicking protein secondary structure elements. *Curr. Top. Med. Chem.* **7**, 33–62
62. Cunningham, A. D., Qvit, N., and Mochly-Rosen, D. (2017) Peptides and peptidomimetics as regulators of protein-protein interactions. *Curr. Opin. Struct. Biol.* **44**, 59–66
63. Davenport, A. P., Scully, C. C. G., de Graaf, C., Brown, A. J. H., and Maguire, J. J. (2020) Advances in therapeutic peptides targeting G protein-coupled receptors. *Nat. Rev. Drug Discov.* **19**, 389–413
64. Muller, P. Y., and Milton, M. N. (2012) The determination and interpretation of the therapeutic index in drug development. *Nat. Rev. Drug Discov.* **11**, 751–761
65. Klauzinska, M., Baljinnyam, B., Raafat, A., Rodriguez-Canales, J., Strizzi, L., Greer, Y. E., Rubin, J. S., and Callahan, R. (2012) Rspo2/Int7 regulates invasiveness and tumorigenic properties of mammary epithelial cells. *J. Cell Physiol.* **227**, 1960–1971
66. Gawantka, V., Delius, H., Hirschfeld, K., Blumenstock, C., and Niehrs, C. (1995) Antagonizing the Spemann organizer: Role of the homeobox gene Xvent-1. *EMBO J.* **14**, 6268–6279